dc electric cloak concentrator via topology optimization

Garuda Fujii [*]
Institute of Engineering, Shinshu University, 4-17-1 Wakasato Nagano 380-8553, Japan

Youhei Akimoto
Faculty of Engineering, Information and Systems, University of Tsukuba & RIKEN AIP, 1-1-1 Tennodai, Tsukuba 305-8573, Japan

(Received 22 May 2020; accepted 19 August 2020; published 10 September 2020)

We succeeded in simultaneously cloaking and concentrating direct current in a conducting material through topology optimization based on a level-set method. To design structures that perform these functions simultaneously, optimal topology is explored for improving two objective functions that govern separately the cloaking and concentration of current. Our design scheme, i.e., the topology optimization of a direct-current electric cloak concentrator, provides this bifunctionality well despite simple, common bulk materials being used to make up the structures. The materials also rigorously obey the electric conduction equation in contrast to the approximated artificial materials, so-called metamaterials, of other design schemes. The structural features needed for this simultaneous bifunctionality are found by adopting level-set method to generate material domains and clear structural interfaces. Furthermore, robust performances of the bifunctional structures against fluctuations in electrical conductivity was achieved by improving the fitness incorporating multiple objective functions. Additionally, the influence of the size of the current-concentrating domain on the performances of the optimal configuration is investigated.

DOI: 10.1103/PhysRevE.102.033308

I. INTRODUCTION

Following the advancements of transformation optics [1,2] and metamaterials [3,4], a variety of innovative devices, collectively called metadevices, were actively developed. Transformation theory and metadevices grew from the field of electromagnetism [1,2] to encompass diverse fields such as acoustics [5], thermotics [6,7], magnetostatics [8,9], and multiphysics [10–13]. The analogy of optical invisibility [14] spread to electronics, where networks constructed of resistors [15] are frequently adopted in developing electric metadevices manipulating electrical direct current (dc) as active cloaks [16], remote cloaks [17,18], carpet cloaks [19], and current concentrators [20]. However, constructing such networks poses difficulties because fabricating the complex resistors needs to be precise to achieve the required properties that have only been estimated approximately. To overcome the fabrication complexity of these metadevices in electrostatics, schemes based on bulk natural materials were proposed such as the bilayer cloak [21,22] for cloaking and the fan-shaped concentrator [21] for concentrating currents. With the use of bulk natural materials rather than resistor networks, design schemes have been strictly determined by the governing equation of electric conduction with the performances of these schemes being more accurately estimated in comparison with those based on approximate schemes. However, electrically conducting metadevices have only a *single* function, such as electrical cloaking or current concentration. The *simultaneous realization* of a multifunctional device for electrical manipulations is still difficult, but multifunctionality is needed for practical realizations of innovative applications such as the invisible sensor [23]. For manipulating thermal conduction, this multifunctionality has been studied not only in theory and experiment [24,25] but also in numerical approaches [26]. Because both voltage and temperature in the steady-state are governed by Laplace's equations, an analogy of multifunctionality for electrical conduction is expected.

In this work, we exploit topology optimization to develop a dc electrical cloak concentrator to open the field of *multifunctional* electrical metadevices. Topology optimization [27] proves to be the most-flexible structural optimization that enables the structural topology of materials to be modified, including the creation during the computational design process of variously shaped pores, and provides an optimal configuration having remarkable performance for any prescribed structural design problem. For the dc electric cloak concentrator to gain this simultaneous bifunctionality, two objective functions must be defined and optimized simultaneously, one for the concentration of the direct current and the other for electrical cloaking [28,29]. To determine the configuration of the structures for this cloak concentrator, a level-set method is employed to generate isosurfaces of the level-set function that defines the interfaces between the different electrical materials. The optimal level-set function (i.e., the optimal configuration) is explored using a covariance matrix adaptation evolution strategy (CMA-ES) [30], which is a robust optimizer that overcomes difficulties such as multimodality, the interdependencies of design variables, and the high ratios of material properties. By employing the CMA-ES, designers

[*] g_fujii@shinshu-u.ac.jp

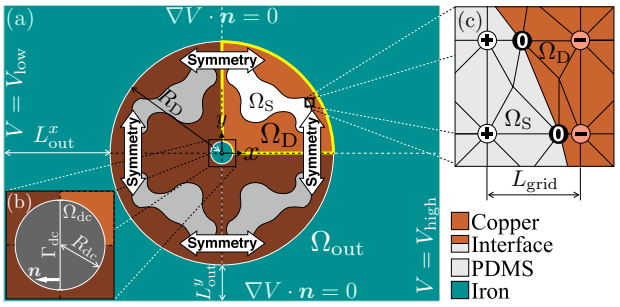

FIG. 1. (a) Schematic of the topology optimization of a dc electric cloak concentrator. All domain sizes are set to $L^x_{\rm out} = R_{\rm D}$ and $L^y_{\rm out} = R_{\rm D}/3$. The conductivities of iron, copper, and PDMS are, respectively, $\sigma_{\rm Fe} = 9.90 \times 10^{-6}$ S/m, $\sigma_{\rm Cu} = 59.0 \times 10^{-6}$ S/m, and $\sigma_{\rm PDMS} = 10^{-5} \times \sigma_{\rm Fe}$. The electrical conductivity of PDMS almost vanishes, and the ersatz material approach [32] in electrostatics is used to determine $\sigma_{\rm PDMS}$. (b) Direct current is concentrated in domain $\Omega_{\rm dc}$ to be comprise of iron, its size being set to $R_{\rm dc} = R_{\rm D}/10$. (c) Discretized level-set functions ϕ_j and their structural expressions showing a clear interface between copper and PDMS; the grid size is set to $L_{\rm grid} = R_{\rm D}/60$.

can reach optimal configurations in topology optimization problem without trial and error concerning both the initial guess of starting configuration and the adjustments parameters available from the strategy [31]. The structural perimeter is minimized with respect to the two objective functions as a perimeter constraint to regularize the ill-posed aspects of this topology optimization problem. The computational demonstration finds structural features that are indispensable for simultaneous electrical cloaking and current concentration. Furthermore, to realize a dc electrical cloak concentrator having a performance that is robust against fluctuations in electrical conductivity, topology optimizations must take into account fluctuations in electrical conductivity.

Several significant advances of the presented studies are as follows: First, simultaneous realization of cloaking and current concentration in an electrical conductor is reported for the first time. Second, the formulation of the optimization problem for simultaneous cloaking and current concentration of an electrical conductor is presented. Third, the topology optimization presented generates optimal configurations of high-performing metadevices using only common bulk materials. Cloaking and current concentration performances have been accurately evaluated through the numerical simulations solving the electrical conduction equation in the steady state. Fourth, key structural features needed for the simultaneous cloaking and concentrating have been identified with clear interfaces generated by the level-set method.

II. FORMULATION

A. Scheme

The scheme for the topology optimization of a dc electric cloak concentrator is illustrated in Fig. 1. To generate a current (from right to left in figure) in the host structure made of iron, low- and high-voltage boundary conditions, $V = V_{\rm low}$ and $V = V_{\rm high}$, are imposed over the left and right boundaries of the host structure, respectively, and an electrically insulated boundary condition, $\nabla V \cdot \boldsymbol{n} = 0$, is imposed over its lower and upper boundaries. The current is concentrated in a small central domain of the iron material, designated $\Omega_{\rm dc}$ in Fig. 1(b). For cloaking, perturbations of the voltage distribution are simultaneously suppressed in the outer domain $\Omega_{\rm out}$. The optimal structure for the simultaneous electrical cloaking and current concentration is configured in the fixed design domain $\Omega_{\rm D}$ in which the optimal layout of materials, specifically, copper and polydimethylsiloxane (PDMS), is explored through structural transforming. The layout of copper and PDMS is determined using the discretized level-set functions [Fig. 1(c)] as design variables on which the objective function being optimized is based. By changing the level-set functions discretized into grid points and their signs ["±" in Fig. 1(c)], the domain $\Omega_{\rm S}$ occupied by PDMS is transformed in the fixed design domain $\Omega_{\rm D}$ and the isosurface of the level-set functions, $\phi(\boldsymbol{x}) = 0$, determining the interface ["0" in Fig. 1(c)], is obtained by linear interpolation of the function in the grids.

B. Objective functions

To enable the simultaneous cloaking and concentration of direct current, two objective functions are considered. For cloaking, perturbations of the voltage distribution are suppressed in $\Omega_{\rm out}$ and the following function is minimized:

$$\Psi_{\rm cloak} = \frac{1}{\Psi^{\rm PDMS}_{\rm cloak}} \int_{\Omega_{\rm out}} |V - V_{\rm Fe}|^2 d\Omega, \tag{1}$$

where V denotes the cloaked distribution of the voltage, $V_{\rm Fe}$ the undisturbed voltage distribution for reference to be reproduced when $\Omega_{\rm D}$ is filled with iron (Fe), and $\Psi^{\rm PDMS}_{\rm cloak}$ the normalization value,

$$\Psi^{\rm PDMS}_{\rm cloak} = \int_{\Omega_{\rm out}} |V_{\rm PDMS} - V_{\rm Fe}|^2 d\Omega, \tag{2}$$

where $V_{\rm PDMS}$ denotes the disturbed voltage when $\Omega_{\rm D}$ is filled with PDMS. Under normalization, the objective function, Eq. (1), becomes $\Psi_{\rm cloak} = 1$ when $\Omega_{\rm D}$ is filled with PDMS. For current concentration, the direct current passing through the plane $\Gamma_{\rm dc}$ in Fig. 1(b) needs to be increased and a second objective function maximized,

$$\Psi_{\rm dc} = \frac{1}{\Psi^{\rm Fe}_{\rm dc}} \int_{\Gamma_{\rm dc}} -\sigma_{\rm dc} \nabla V \cdot \boldsymbol{n}\, d\Gamma, \tag{3}$$

where $\sigma_{\rm dc}$ denotes the electrical conductivity of the material occupying $\Omega_{\rm dc}$, $\boldsymbol{n}$ the unit normal vector on $\Gamma_{\rm dc}$, and $\Psi^{\rm Fe}_{\rm dc}$ the value for normalization defined as

$$\Psi^{\rm Fe}_{\rm dc} = \int_{\Gamma_{\rm dc}} -\sigma_{\rm Fe} \nabla V_{\rm Fe} \cdot \boldsymbol{n}\, d\Gamma, \tag{4}$$

where $\sigma_{\rm Fe}$ denotes the electrical conductivity of iron. When $\Omega_{\rm D}$ is filled with iron, the normalized value of the objective function for current concentration becomes $\Psi_{\rm dc} = 1$.

C. Governing equation and design variable

The voltage in the steady state is governed by Laplace's equations,

$$\nabla \cdot (\sigma(\boldsymbol{x})\nabla V) = 0,$$

where $\sigma(\boldsymbol{x})$ denotes the position-dependent electrical conductivity given as

$$\sigma(\boldsymbol{x}) = \begin{cases} \sigma_{\mathrm{Cu}} + \chi(\sigma_{\mathrm{PDMS}} - \sigma_{\mathrm{Cu}}) & \text{for } \boldsymbol{x} \in \Omega_{\mathrm{D}} \\ \sigma_{\mathrm{Fe}} & \text{for } \boldsymbol{x} \in \Omega_{\mathrm{out}}, \Omega_{\mathrm{dc}} \end{cases},$$

where σ_{Cu}, σ_{PDMS}, and σ_{Fe} denote the electrical conductivities of copper, PDMS, and iron, respectively. The electrical conductivity of PDMS is almost zero; a sufficiently small value is assigned to it, as in the ersatz material approach [32] in electrostatics. The characteristic function χ is defined as

$$\chi(\phi(\boldsymbol{x})) = \begin{cases} 1 & \text{if } \boldsymbol{x} \in \Omega_{\mathrm{S}} \\ 0 & \text{if } \boldsymbol{x} \in \Omega_{\mathrm{D}} \backslash \Omega_{\mathrm{S}} \end{cases},$$

where $\phi(\boldsymbol{x})$ denotes the level-set function that determines the domains and their interfaces,

$$\begin{aligned} \Omega_{\mathrm{S}} \backslash \Gamma_{\mathrm{S}} &= \{\boldsymbol{x} \mid 0 < \phi(\boldsymbol{x}) \leqslant 1\}, \\ \Gamma_{\mathrm{S}} &= \{\boldsymbol{x} \mid \phi(\boldsymbol{x}) = 0\}, \\ \Omega_{\mathrm{D}} \backslash \Omega_{\mathrm{S}} &= \{\boldsymbol{x} \mid -1 \leqslant \phi(\boldsymbol{x}) < 0\}, \end{aligned}$$

where Ω_{S} denotes the domain occupied by PDMS, $\Omega_{\mathrm{D}} \backslash \Omega_{\mathrm{S}}$ the fixed design domain excluding Ω_{S} and occupied by copper, and Γ_{S} the interfaces between copper and PDMS. The level-set function is a continuous function of the design variable that is then discretized onto grid points in the optimization computation as $\boldsymbol{\phi} = \{\phi_1, \ldots, \phi_j, \ldots, \phi_n\}$ [see Fig. 1(c)].

D. Regularization and fitness

Because the optimization problem is ill posed in that it allows an optimal configuration containing infinitely fine structures, topology optimization must include relaxation or regularization. For the present topology optimization based on the level-set method, a perimeter constraint is employed in which the structural perimeter L_{p} is minimized along with the objective functions. We define the fitness function composed of a minimized Ψ_{cloak}, maximized Ψ_{dc}, and minimized L_{p}; specifically,

$$\inf_{\phi} \quad F_{\mathrm{r}} = \Psi_{\mathrm{cloak}} + \left(\frac{1}{\Psi_{\mathrm{dc}}}\right)^{p} + \tau L_{\mathrm{p}}, \tag{5}$$

where p denotes the multiplier of the Ψ_{dc} reciprocal to change the priority between minimizing Ψ_{cloak} and maximizing Ψ_{dc} (i.e., cloaking and concentration of direct current), and τ is the regularization coefficient that establishes the ratio of the performances of Ψ_{cloak} and Ψ_{dc} to that of the perimeter L_{p}. In the numerical demonstration described below, we set $p = 4$ and vary τ to generate several cases for design. The optimum $\boldsymbol{\phi}$ is explored by the CMA-ES [30] with the handling of the box constraint [31], $-1 \leqslant \phi_j \leqslant 1$, to improve the regularized fitness function F_{r}. For more details, see Refs. [31,33,34].

III. RESULTS

A. Unperturbed voltage distribution for reference and the distribution perturbed by introducing PDMS

The homogeneous electrical system made of iron and the undisturbed voltage distribution are shown in Fig. 2(a) and 2(b), respectively. The fixed design domain Ω_{D} is filled with iron [see Fig. 2(a)] and the contour lines of the distribution become straight without any perturbation in the voltage distribution [see Fig. 2(b)]. The homogeneous system provides an ideal distribution for cloaking, and the voltage V corresponds to V_{Fe}; hence, the difference $V - V_{\mathrm{Fe}}$ vanishes as $V_{\mathrm{Fe}} - V_{\mathrm{Fe}} = 0$ everywhere in the system [Fig. 2(c)]. The value of the objective function for cloaking is ideal as $\Psi_{\mathrm{cloak}} = 0$; in contrast, no function for the current concentration is realized, as evident in Fig. 2(d). For comparison, the value of the objective function for current concentration in this system becomes one under normalization Eq. (3); i.e., $\Psi_{\mathrm{dc}} = 1$.

We also show the perturbed distribution of the voltage in Figs. 2(e)–2(h) obtained by filling Ω_{D} with PDMS. The domain of the current concentration Ω_{dc} is surrounded by electrical insulating material PDMS [Fig. 2(e)]; the contour lines of the voltage distribution are largely bent by the PDMS [Fig. 2(f)]. Because the perturbation of the voltage is large, the difference evaluated for cloaking, $V - V_{\mathrm{Fe}} = V_{\mathrm{PDMS}} - V_{\mathrm{Fe}}$, is obvious [Fig. 2(g)], and the value of the objective function for cloaking is set to $\Psi_{\mathrm{cloak}} = 1$ under normalization, Eq. (1). The direct current flows around the PDMS [Fig. 2(h)] and the objective function for current concentration becomes very small as $\Psi_{\mathrm{dc}} = 3.62 \times 10^{-5}$.

B. Topology-optimized dc electric cloak concentrator

The structural transformation of the dc electric cloak concentrator during the present topology optimization is shown in Fig. 3. As the generation of the CMA-ES proceeds from $g = 0$, fine structures in the configurations develop through the perimeter constraint imposed in the fitness function, Eq. (5). Finally, by adjusting the regularization coefficient τ, optimal configurations were obtained having different structural complexity [rightmost in Fig. 3]. Large τ, for example, $\tau = 1 \times 10^{-2}$ [Fig. 3(a)], produce simple and easy-to-fabricate optimal configurations because the perimeter constraint is strong. Indeed, for $\tau = 1 \times 10^{-2}$, the perimeter of the optimal configuration is $L_{\mathrm{p}} = 5.72$, which is much less than $L_{\mathrm{p}} = 22.2$ with small $\tau = 1 \times 10^{-4}$ [Fig. 3(c)] yielding optimal configurations that are poorly manufacturable with complex curved interfaces between copper and PDMS with the weaker constraint. With small values of τ, performance dominates in simplifying the configuration, and hence the optimization aggressively improves the performance rather than improves manufacturability of the configuration.

Figure 4 shows the optimal configurations with its characteristics and the performances of these optimal configurations. The voltage distributions in Figs. 4(b), 4(f) and 4(j) are altered as the cloak concentrator is optimized with the contour lines of the voltages becoming almost completely straight in Ω_{out}. The difference $V - V_{\mathrm{Fe}}$ used in determining the cloaking capability is given in Figs. 4(c), 4(g) and 4(k) at a fine scale,

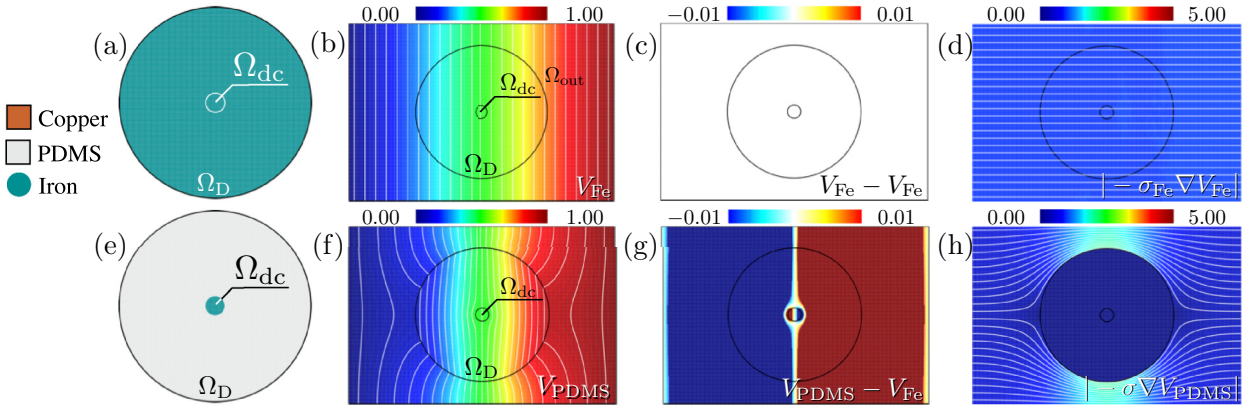

FIG. 2. Results when Ω_D is filled with [(a)–(d)] iron and [(e)–(h)] PDMS for reference and normalizations. [(a) and (e)] Configuration in Ω_D, [(b) and (f)] voltage distribution with contours, [(c) and (g)] evaluated difference of voltages and the objective function value for cloaking, [(d) and (h)] the magnitude (color) and direction (streamline) of the direct current and the value of the objective function for current concentration. The values of the objective functions are [(a)–(d)] $\Psi_{cloak} = 0.00 \times 10^0$ and $\Psi_{dc} = 1.00 \times 10^0$ and [(e)–(f)] $\Psi_{cloak} = 1.00 \times 10^0$ and $\Psi_{dc} = 3.62 \times 10^{-5}$.

$-0.01 \leqslant V - V_{Fe} \leqslant 0.01$, to emphasize the cloaking performance. The cloaking performance significantly improves as the value of the regularization coefficient τ diminishes; the voltage difference becomes almost completely zero everywhere in Ω_{out} [Fig. 4(k)] as evident in the magnified plot. Moreover, the current concentration performance is also improved [Figs. 4(d), 4(h) and 4(l)]; the magnitude and direction of the direct current are plotted using a color scale and streamlines, respectively. For the optimal configurations, the values of the objective function for current concentration, Ψ_{dc}, are given in the caption of Fig. 4. The direct current is bent and concentrated into Ω_{dc} by funnel-shaped structures made of PDMS located above and below Ω_{dc}.

In the left close-ups of Figs. 4(d), 4(h) and 4(l), unconcentrated direct current represented as streamlines bypasses the funnel-like structures and pass through the narrow copper structures between the funnel-like PDMS domains and host domains of iron. The narrow copper structures shown in the

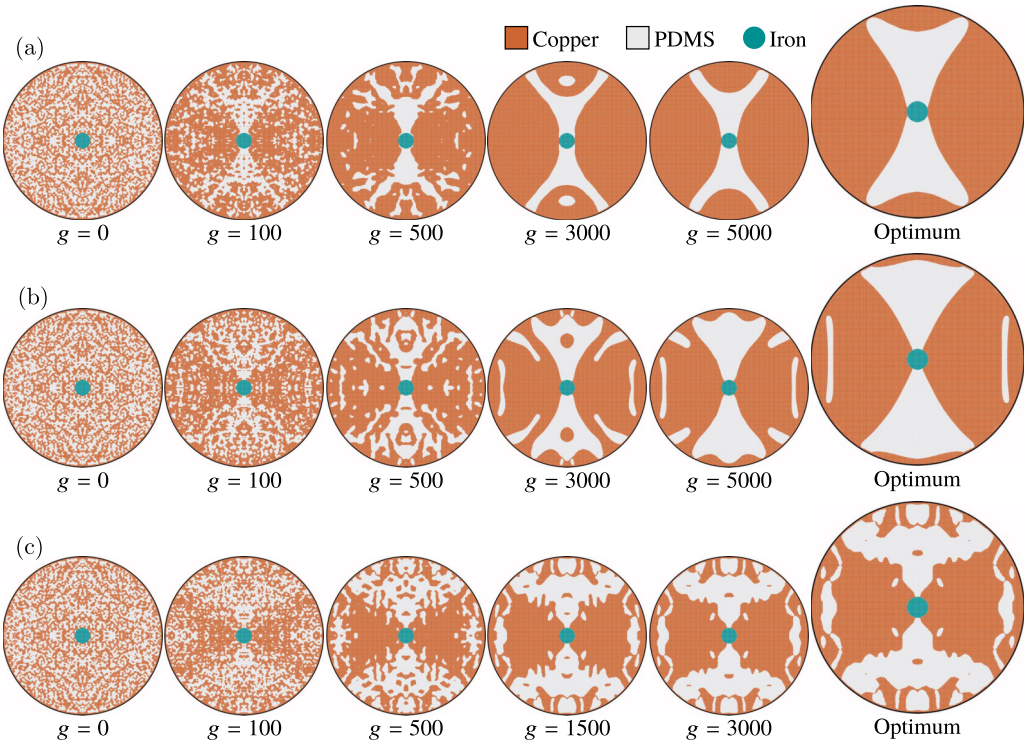

FIG. 3. The structural transformation of the dc electric cloak concentrator obtained under (a) $\tau = 1 \times 10^{-2}$, (b) $\tau = 1 \times 10^{-3}$, and (c) $\tau = 1 \times 10^{-4}$. Structural perimeter; the total interface length between copper and PDMS in the optimal configuration becomes (a) $L_p = 5.72$, (b) $L_p = 9.43$, and (c) $L_p = 22.2$. Each structure corresponds to the smallest F_r value from 140 samples in each generation g.

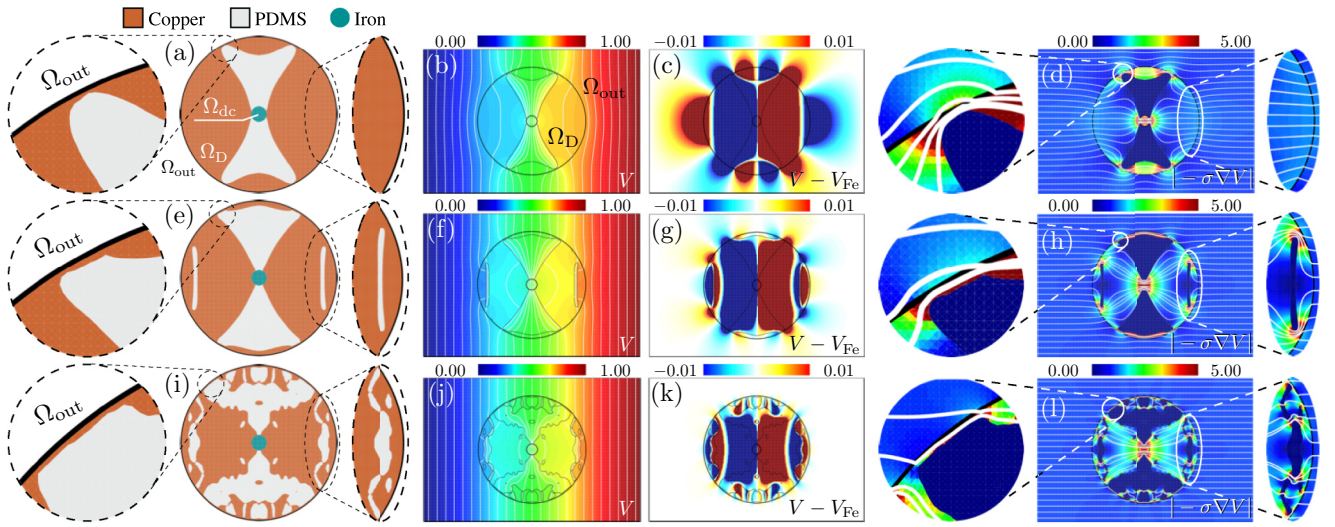

FIG. 4. Optimal configurations and the performances of the optimal configurations obtained setting [(a)–(d)] $\tau = 1 \times 10^{-2}$, [(e)–(h)] $\tau = 1 \times 10^{-3}$, and [(i)–(l)] $\tau = 1 \times 10^{-4}$. [(a), (e), and (i)] Optimal configuration in Ω_D, its characteristics viewed in close-ups, and perimeter of the optimal configuration. [(b), (f), and (i)] Voltage distribution with contours when the optimal configuration is present, [(c), (g), and (k)] evaluated difference of voltages and the value of the objective function for cloaking, and [(d), (h), and (l)] magnitude (color scale) and direction (streamlines) of the direct current and the value of the objective functional for current concentration. The values of the objective functions and the perimeter are [(a)–(d)] $\Psi_{cloak} = 8.11 \times 10^{-3}$, $\Psi_{dc} = 4.48 \times 10^{0}$, and $L_p = 5.72$; [(e)–(f)] $\Psi_{cloak} = 7.70 \times 10^{-4}$, $\Psi_{dc} = 6.42 \times 10^{0}$, and $L_p = 9.43$; [(i)–(l)] $\Psi_{cloak} = 3.35 \times 10^{-5}$, $\Psi_{dc} = 7.10 \times 10^{0}$, and $L_p = 22.2$.

left close-ups of Figs. 4(a), 4(e) and 4(i) function as a passage of unconcentrated direct current to suppress the perturbation of the outer voltage distribution for cloaking. We also find *barrier* structures shown in right close-ups of Figs. 4(e) and 4(i). These structures prevent excessive direct current flowing in and out of Ω_{dc} to keep the outer voltage perturbations suppressed for cloaking while actively concentrating the current. They emerge only in the optimum configurations under weaker perimeter constraints with settings $\tau = 1 \times 10^{-3}$ and $\tau = 1 \times 10^{-4}$ [right close-ups of Figs. 4(e) and 4(i)].

The proposed cloak concentrator is expected to be applied in invisible sensing [23,35] with the electrical conductivity of the concentration domain, σ_{dc}, changed from that of iron, σ_{Fe}, when the domain σ_{dc} is placed in an electrical sensor. We investigated the performance dependence of optimal cloak concentrators on σ_{dc}; the dependencies for electrical cloaking and current concentration are shown in Figs. 5(a) and 5(b), respectively. The horizontal axis shows the electrical conductivity of the concentration domain Ω_{dc} normalized by that of the host Ω_{out}. The topology optimizations presented in Figs. 3 and 4 were generated under $\sigma_{dc}/\sigma_{host} = \sigma_{Fe}/\sigma_{Fe} = 1$. Whereas the current concentration performance exhibits a low dependence on the fluctuation of σ_{dc} [Fig. 5(b)], the performance for cloaking depends strongly on σ_{dc} [Fig. 5(a)]. A higher σ_{dc} guides the excess direct current flowing in and out of Ω_{dc}; an excessively concentrated current perturbs the outer voltage distribution, thereby degrading the cloaking performance. A lower σ_{dc} suppresses current flowing into Ω_{dc} and that also perturbs the outer distribution of the voltage.

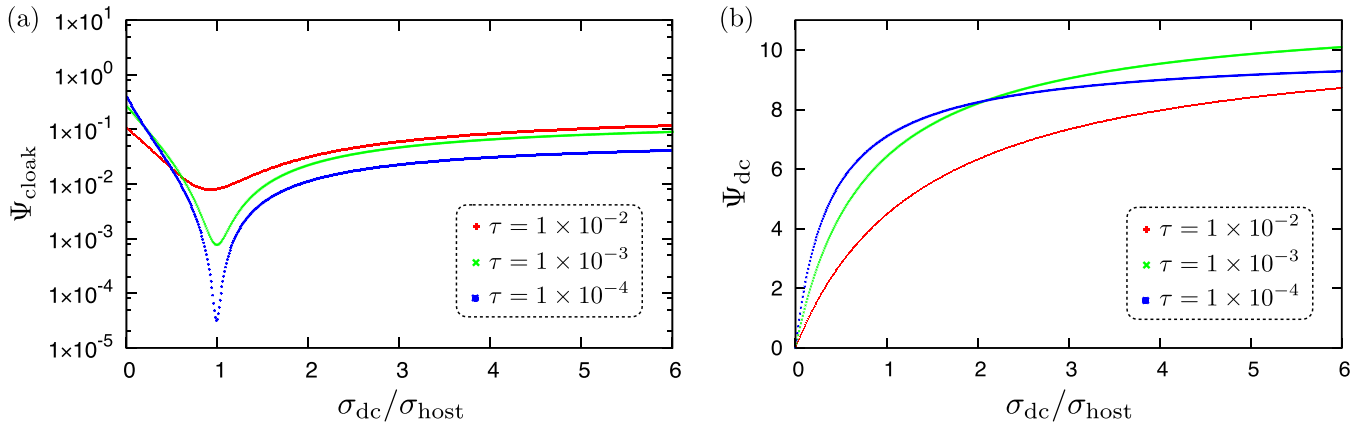

FIG. 5. Performance dependence of the concentration domain Ω_{dc} on the electrical conductivity. (a) Cloaking performance versus conductivity in Ω_{dc}. (b) Concentrating performance versus conductivity in Ω_{dc}. The conductivity of the host material is fixed at $\sigma_{host} = \sigma_{Fe}$ and the normalization values for Ψ_{cloak}^{PDMS} and Ψ_{dc}^{Fe} are fixed by Eqs. (2) and (4), respectively.

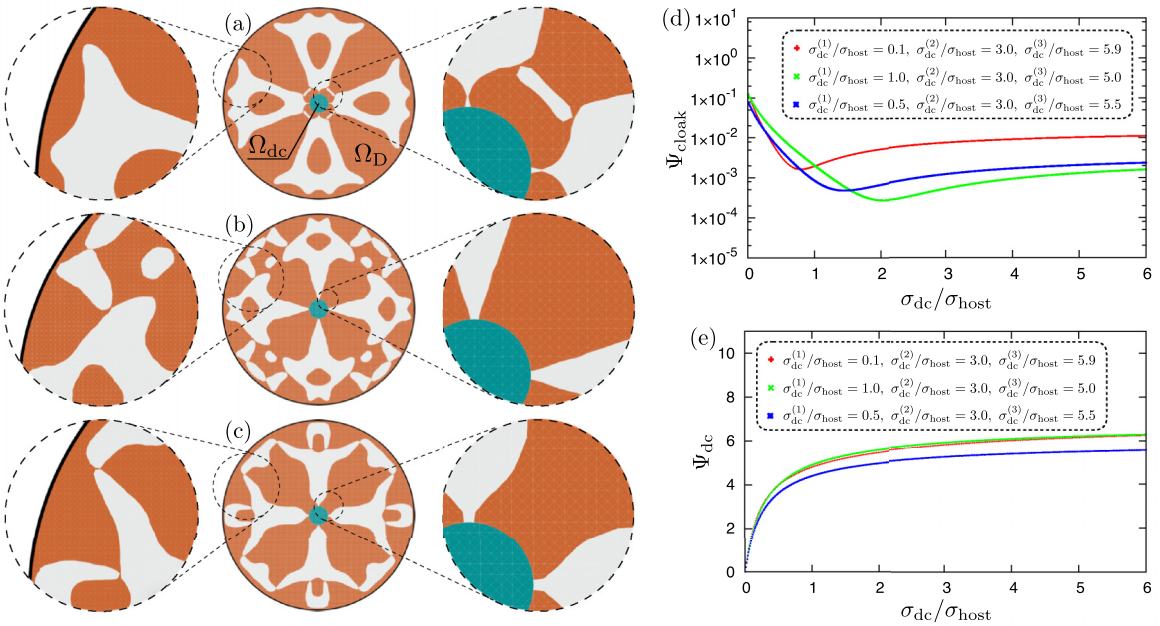

FIG. 6. Optimization results obtained by minimizing $F_{\rm rbst}$ for three values of the electrical conductivity $\sigma_{\rm dc}$. Optimal configurations are obtained for (a) $\sigma_{\rm dc}^{(1)}/\sigma_{\rm host} = 0.1$, $\sigma_{\rm dc}^{(2)}/\sigma_{\rm host} = 3.0$, and $\sigma_{\rm dc}^{(3)}/\sigma_{\rm host} = 5.9$; (b) $\sigma_{\rm dc}^{(1)}/\sigma_{\rm host} = 1.0$, $\sigma_{\rm dc}^{(2)}/\sigma_{\rm host} = 3.0$, and $\sigma_{\rm dc}^{(3)}/\sigma_{\rm host} = 5.0$; and (c) $\sigma_{\rm dc}^{(1)}/\sigma_{\rm host} = 0.5$, $\sigma_{\rm dc}^{(2)}/\sigma_{\rm host} = 3.0$, and $\sigma_{\rm dc}^{(3)}/\sigma_{\rm host} = 5.5$. The number of samplings is set to 140. The settings for the regularization coefficient and multiplier are $\tau = 1 \times 10^{-3}$ and $p = 4$.

C. Multidirectional dc electric cloak concentrator robust to fluctuation of electrical conductivity

The performance of a cloak concentrator exhibits a strong dependence on the electrical conductivity in $\Omega_{\rm dc}$ (Fig. 5). To reduce this dependence and improve the robustness of the performance against fluctuations in electrical conductivity $\sigma_{\rm dc}$, a topology optimization that takes into account such fluctuations was conducted. The objective functions were computed for three values of $\sigma_{\rm dc}$ and a fitness function incorporating the objective functions for various $\sigma_{\rm dc}$ values was employed,

$$\inf_{\phi} \quad F_{\rm rbst} = \frac{1}{3}\sum_{i=1}^{3}\left(\Psi_{\rm cloak}\left(\sigma_{\rm dc}^{(i)}\right) + \left(\frac{1}{\Psi_{\rm dc}\left(\sigma_{\rm dc}^{(i)}\right)}\right)^{p}\right) + \tau L_{\rm p},$$

where $\Psi_{\rm cloak}(\sigma_{\rm dc}^{(i)})$ and $\Psi_{\rm dc}(\sigma_{\rm dc}^{(i)})$ denote, respectively, the objective functions for cloaking and concentration under electrical conductivity $\sigma_{\rm dc}^{(i)}$, with i an indexing of the objective functions. Simultaneous cloaking and concentration of direct current for three distinct $\sigma_{\rm dc}$ values were realized by minimizing $F_{\rm rbst}$. We improved not only the robustness of the performance of each cloak concentrator but also the directionality of the cloaking and current concentration by implementing structural symmetries about the x and y axes and diagonals $y = \pm x$. These cloak concentrators in Fig. 4 were optimized to manipulate direct current directed only towards the negative x axis; the symmetries increased the direction of the current over the domain in which the cloak concentrator functions.

Figures 6(a)–6(c) shows the optimization results obtained under several sets of $\sigma_{\rm dc}^{(i)}$, and Figs 6(d) and 6(e) display the performance robustness for cloaking and current concentration. The dependence of the cloaking performance on $\sigma_{\rm dc}$ [Fig. 6(d)] is obviously reduced by incorporating multiple $\sigma_{\rm dc}^{(i)}$ in the topology optimizations. Performances at high conductivity $1 < \sigma_{\rm dc}/\sigma_{\rm host}$ are significantly improved compared with those of the previous topology optimizations [Fig. 5(a)]. In particular, the performance obtained under $\sigma_{\rm dc}^{(i)}/\sigma_{\rm host} = 0.5, 3.0, 5.5$ in Fig. 6(d) exhibits robustness not only at high conductivity but also at low conductivity. The concentration domain $\Omega_{\rm dc}$ is surrounded by PDMS in *almost* all directions, and only narrow copper structures remain in some places between the PDMS domains [right close-up of Fig. 6(a) and left close-ups of Figs. 6(b) and 6(c)]. To achieve a robust cloaking performance, it is necessary to surround $\Omega_{\rm dc}$ with PDMS in *almost* all directions to reduce the influence of the $\sigma_{\rm dc}$ fluctuations on the outer voltage distribution. Indeed, the cloaking performance shown in Fig. 6(d) is less affected by fluctuations in $\sigma_{\rm dc}$. However, if the $\sigma_{\rm dc}$ is *completely* surrounded with PDMS, then the direct current cannot be concentrated, necessitating a thin copper structure to remain. Therefore, the current-concentration performance does not largely improve but becomes robust despite increases in $\sigma_{\rm dc}$ [Fig. 6(e)].

D. Influence of the size of the concentrating domain on performance

The demonstrated topology optimizations shown above assume rather small-sized $\Omega_{\rm dc}$. We investigate the influence of the size of $\Omega_{\rm dc}$ on the performance of the topology optimized-dc electrical cloak concentrator. Figure 7(a) shows the relationship between the radius of $\Omega_{\rm dc}$ and the cloaking performance (left vertical axis) of the optimal configurations obtained and that between the radius and the concentrating performance (right vertical axis) of the optimal configurations. Both performances tend to worsen as the size of $\Omega_{\rm dc}$ increases.

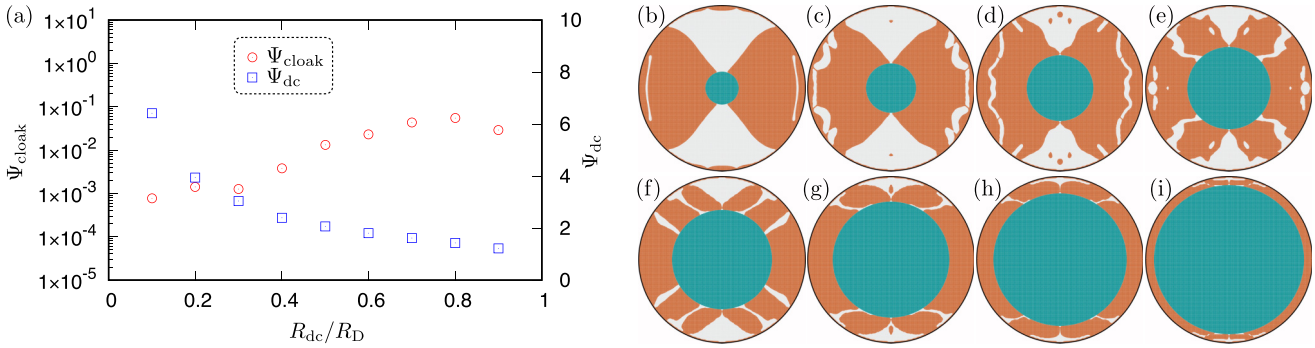

FIG. 7. (a) Dependence of the performances on the domain-size for the concentration. [(b)–(i)] Optimal configurations obtained for (b) $R_{\rm dc}/R_{\rm D} = 0.2$, (c) 0.3, (d) 0.4, (e) 0.5, (f) 0.6, (g) 0.7, (h) 0.8, and (i) 0.9 under $\tau = 1 \times 10^{-3}$.

However, the objective functions given in Eqs. (1) and (3) are defined by comparing the performances of the cloak concentrator with that of an electric system without cloak concentrator. In particular, $\Psi_{\rm dc}$ in Eq. (3) experiences a large influence from variations in $R_{\rm dc}$ because the value of $\Psi_{\rm dc}^{\rm Fe}$ used for the normalization in Eq. (3) strongly depends on the area of the phase $\Gamma_{\rm dc}$. In contrast to the strong dependency of $\Psi_{\rm dc}^{\rm Fe}$ on $R_{\rm dc}$, the value of $\Psi_{\rm cloak}^{\rm PDMS}$ has low dependence on $R_{\rm dc}$ variation because $\Omega_{\rm dc}$ is surrounded by low-conductive PDMS. To compare the efficiency of the concentrating dc under different $R_{\rm dc}$, we employ an alternative value that does not depend on $R_{\rm dc}$ for normalizing the evaluating dc concentration in the following:

$$\Psi_{\rm D}^{\rm Fe} = \int_{\Gamma_{\rm D}} -\sigma_{\rm Fe} \nabla V_{\rm Fe} \cdot \boldsymbol{n}\, d\Gamma,$$

where $\Gamma_{\rm D}$ is a plane along the y axis that crosses the fixed design domain $\Omega_{\rm D}$ [see Fig. 8(b)]. Then $\Psi_{\rm D}^{\rm Fe}$ represents all dc passing through $\Omega_{\rm D}$ when the Fe-made homogeneous electrical system is present without the cloak concentrator. We note that the difference between $\Psi_{\rm D}^{\rm Fe}$ and $\Psi_{\rm dc}^{\rm Fe}$ is the area where the passing current is integrated along and satisfies the following relation as

$$\frac{\Psi_{\rm D}^{\rm Fe}}{\Psi_{\rm dc}^{\rm Fe}} = \frac{R_{\rm D}}{R_{\rm dc}}.$$

With this normalization by $\Psi_{\rm D}^{\rm Fe}$, we introduce another index to evaluate the efficiency in concentrating dc, specifically,

$$\Psi_{\rm eff} = \frac{1}{\Psi_{\rm D}^{\rm Fe}} \int_{\Gamma_{\rm dc}} -\sigma_{\rm dc} \nabla V \cdot \boldsymbol{n}\, d\Gamma,$$
$$= \frac{R_{\rm dc}}{R_{\rm D}} \Psi_{\rm dc}.$$

The above $\Psi_{\rm eff}$ shows concentrated dc passing through the concentration domain $\Gamma_{\rm dc}$ compared with that through the fixed design domain $\Gamma_{\rm D}$. When electrical systems are cloaked *perfectly* with no disturbance in the outer voltage, the maximum $\Psi_{\rm eff}$ becomes 1.

Figure 8(a) shows the relationship between $\Psi_{\rm eff}$ and the size of $\Omega_{\rm dc}$. We also plot $\Psi_{\rm dc}$ for comparison in Fig. 8(a). As $R_{\rm dc}$ increases, the efficiency of the concentrating $\Psi_{\rm eff}$ is enhanced despite $\Psi_{\rm dc}$ becoming smaller. This trend shows that we need to consider the influence of $R_{\rm dc}$ on $\Psi_{\rm dc}$ in comparing the concentrating performance of optimal configurations obtained for different $R_{\rm dc}$. In some cases with $R_{\rm dc}/R_{\rm D} \geqslant 0.5$, $\Psi_{\rm eff}$ is over 1 and sufficient concentrating performance is exhibited. However, $\Psi_{\rm eff} > 1$ means that an excessive dc is concentrated in $\Omega_{\rm dc}$. Actually, the cloaking performance in Fig. 7(a) deteriorates as $R_{\rm dc}$ increases and the excessively concentrated dc causes a voltage disturbance in the outer domain $\Omega_{\rm out}$.

IV. CONCLUSION

The simultaneous cloaking and concentration of direct current was numerically achieved through a topology optimization of a dc electric cloak concentrator. The formulation, numerical results, and improvements in robustness for simultaneous cloaking and current concentration were presented with demonstrations of configurations generated through topology optimization. The optimal configurations obtained performed well as both cloak and concentrator and exhibited specific structural features: funnel-like structures for concentrating the direct current into a central domain and narrow passages and barriers for cloaking the concentrator from the direct current so that the outer voltage distribution is perturbed less. Topology optimization that established a robust performance provided optimal configurations that balanced reducing the conductive fluctuations of the outer voltage and

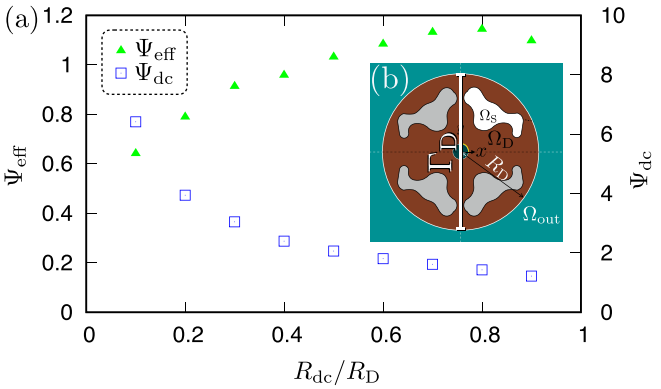

FIG. 8. Dependence of the efficiency of concentrating on the domain size for the concentration.

concentrating the direct current. Moreover, the performance dependence of the optimal dc electric cloak concentrator on the domain size for the concentration was investigated. Our approach is expected to be applied to not only electrical devices but also multiphysical metadevices [12,35].

ACKNOWLEDGMENTS

We acknowledge JSPS Grant-in-Aid for Young Scientists (B) Grant No. 17K17778. We thank Richard Haase from Edanz Group for editing a draft of this manuscript.

[1] U. Leonhardt, Optical conformal mapping, Science **312**, 1777 (2006).
[2] J. B. Pendry, D. Schurig, and D. R. Smith, Controlling electromagnetic fields, Science **312**, 1780 (2006).
[3] J. B. Pendry, A. J. Holden, D. J. Robbins, and W. J. Stewart, Magnetism from conductors and enhanced nonlinear phenomena, IEEE Trans. Microw. Theory Techn. **47**, 2075 (1999).
[4] D. R. Smith, W. J. Padilla, D. C. Vier, S. C. Nemat-Nasser, and S. Schultz, Composite Medium with Simultaneously Negative Permeability and Permittivity, Phys. Rev. Lett. **84**, 4184 (2000).
[5] S. A. Cummer and D. Schurig, One path to acoustic cloaking, New J. Phys. **9**, 45 (2007).
[6] C. Z. Fan, Y. Gao, and J. P. Huang, Shaped graded materials with an apparent negative thermal conductivity, Appl. Phys. Lett. **92**, 251907 (2008).
[7] Y. Li, X. Shen, Z. Wu, J. Huang, Y. Chen, Y. Ni, and J. Huang, Temperature-Dependent Transformation Thermotics: From Switchable Thermal Cloaks to Macroscopic Thermal Diodes, Phys. Rev. Lett. **115**, 195503 (2015).
[8] J. Zhu, W. Jiang, Y. Liu, G. Yin, J. Yuan, S. He, and Y. Ma, Three-dimensional magnetic cloak working from d.c. to 250 khz, Nat. Commun. **6**, 8931 (2015).
[9] W. Jiang, Y. Ma, and S. He, Static Magnetic Cloak without a Superconductor, Phys. Rev. Appl. **9**, 054041 (2018).
[10] J. Y. Li, Y. Gao, and J. P. Huang, A bifunctional cloak using transformation media, J. Appl. Phys. **108**, 074504 (2010).
[11] M. Moccia, G. Castaldi, S. Savo, Y. Sato, and V. Galdi, Independent Manipulation of Heat and Electrical Current via Bifunctional Metamaterials, Phys. Rev. X **4**, 021025 (2014).
[12] Y. Ma, Y. Liu, M. Raza, Y. Wang, and S. He, Experimental Demonstration of a Multiphysics Cloak: Manipulating Heat Flux and Electric Current Simultaneously, Phys. Rev. Lett. **113**, 205501 (2014).
[13] G. Fujii and Y. Akimoto, Optimizing the structural topology of bifunctional invisible cloak manipulating heat flux and direct current, Appl. Phys. Lett. **115**, 174101 (2019).
[14] A. Alù and N. Engheta, Achieving transparency with plasmonic and metamaterial coatings, Phys. Rev. E **72**, 016623 (2005).
[15] F. Yang, Z. L. Mei, T. Y. Jin, and T. J. Cui, Dc Electric Invisibility Cloak, Phys. Rev. Lett. **109**, 053902 (2012).
[16] Q. Ma, Z. L. Mei, S. K. Zhu, T. Y. Jin, and T. J. Cui, Experiments on Active Cloaking and Illusion for Laplace Equation, Phys. Rev. Lett. **111**, 173901 (2013).
[17] F. Yang, Z. L. Mei, X. Y. Yang, T. Y. Jin, and T. J. Cui, A negative conductivity material makes a dc invisibility cloak hide an object at a distance, Adv. Funct. Mater. **23**, 4306 (2013).
[18] T. Chen, B. Zheng, Y. Yang, L. Shen, Z. Wang, F. Gao, E. Li, Y. Luo, T. J. Cui, and H. Chen, Direct current remote cloak for arbitrary objects, Light Sci. Appl. **8**, 30 (2019).
[19] Z. L. Mei, Y. S. Liu, F. Yang, and T. J. Cui, A dc carpet cloak based on resistor networks, Opt. Express **20**, 25758 (2012).
[20] W. X. Jiang, C. Y. Luo, H. F. Ma, Z. L. Mei, and T. J. Cui, Enhancement of current density by DC electric concentrator, Sci. Rep. **2**, 956 (2012).
[21] T. Han, H. Ye, Y. Luo, S. P. Yeo, J. Teng, S. Zhang, and C.-W. Qiu, Manipulating DC currents with bilayer bulk natural materials, Adv. Mater. **26**, 3478 (2014).
[22] T. Han and C.-W. Qiu, Transformation Laplacian metamaterials: Recent advances in manipulating thermal and dc fields, J. Opt. **18**, 044003 (2016).
[23] A. Alù and N. Engheta, Cloaking a Sensor, Phys. Rev. Lett. **102**, 233901 (2009).
[24] S. Narayana and Y. Sato, Heat Flux Manipulation with Engineered Thermal Materials, Phys. Rev. Lett. **108**, 214303 (2012).
[25] X. Shen, Y. Li, C. Jiang, Y. Ni, and J. Huang, Thermal cloak-concentrator, Appl. Phys. Lett. **109**, 031907 (2016).
[26] G. Fujii and Y. Akimoto, Cloaking a concentrator in thermal conduction via topology optimization, Int. J. Heat Mass Transf. **159**, 120082 (2020).
[27] M. P. Bendsøe and N. Kikuchi, Generating optimal topologies in structural design using a homogenization method, Comput. Meth. Appl. Mech. Eng. **71**, 197 (1988).
[28] G. Fujii, Y. Akimoto, and M. Takahashi, Direct-current electric invisibility through topology optimization, J. Appl. Phys. **123**, 233102 (2018).
[29] G. Fujii and Y. Akimoto, DC carpet cloak designed by topology optimization based on covariance matrix adaptation evolution strategy, Opt. Lett. **44**, 2057 (2019).
[30] N. Hansen and A. Ostermeier, Completely derandomized self-adaptation in evolution strategies, Evol. Comput. **9**, 159 (2001).
[31] G. Fujii, M. Takahashi, and Y. Akimoto, CMA-ES-based structural topology optimization using a level set boundary expression—Application to optical and carpet cloaks, Comput. Meth. Appl. Mech. Engng. **332**, 624 (2018).
[32] G. Allaire, F. Jouve, and A. Toader, Structural optimization using sensitivity analysis and a level-set method, J. Comput. Phys. **194**, 363 (2004).
[33] N. Hansen, The CMA evolution strategy: A tutorial, arXiv:1604.00772 (2016).
[34] G. Fujii and Y. Akimoto, Topology-optimized thermal carpet cloak expressed by an immersed-boundary level-set method via a covariance matrix adaptation evolution strategy, Int. J. Heat Mass Trans. **137**, 1312 (2019).
[35] T. Yang, X. Bai, D. Gao, L. Wu, B. Li, J. T. L. Thong, and C.-W. Qiu, Invisible sensors: Simultaneous sensing and camouflaging in multiphysical fields, Adv. Mater. **27**, 7752 (2015).